Published in final edited form as:
Nat Genet. 2002 January ; 30(1): 110–116. doi:10.1038/ng811.

Positional cloning of the combined hyperlipidemia gene *Hyplip1*

Jackie S. Bodnar[1], **Aurobindo Chatterjee**[2], **Lawrence W. Castellani**[1], **David A. Ross**[2], **Jeffrey Ohmen**[2], **James Cavalcoli**[2], **Chenyan Wu**[2], **Katherine M. Dains**[2], **Joe Catanese**[2], **Michael Chu**[1], **Sonal S. Sheth**[1], **Kanti Charugundla**[1], **Peter Demant**[3], **David B. West**[2], **Pieter de Jong**[2], and **Aldons J. Lusis**[1]

[1]Molecular Biology Institute and Departments of Medicine, Human Genetics, and Microbiology, Immunology and Molecular Genetics, University of California, Los Angeles, 47-123 CHS, UCLA School of Medicine, Los Angeles, California 90095, USA [2]Department of Molecular Science, Pfizer Global Research and Development, Ann Arbor Laboratories, Pfizer Inc., Ann Arbor, Michigan 48105, USA [3]Division of Molecular Genetics, The Netherlands Cancer Institute, Amsterdam, The Netherlands

Abstract

Familial combined hyperlipidemia (FCHL, MIM-144250) is a common, multifactorial and heterogeneous dyslipidemia predisposing to premature coronary artery disease[1–2] and characterized by elevated plasma triglycerides, cholesterol, or both[3–4]. We identified a mutant mouse strain, HcB-19/*Dem* (HcB-19), that shares features with FCHL, including hypertriglyceridemia, hypercholesterolemia, elevated plasma apolipoprotein B and increased secretion of triglyceride-rich lipoproteins[5]. The hyperlipidemia results from spontaneous mutation at a locus, *Hyplip1*, on distal mouse chromosome 3 in a region syntenic with a 1q21–q23 FCHL locus identified in Finnish, German, Chinese and US families[6–8]. We fine-mapped *Hyplip1* to roughly 160 kb, constructed a BAC contig and sequenced overlapping BACs to identify 13 candidate genes. We found substantially decreased mRNA expression for thioredoxin interacting protein (*Txnip*). Sequencing of the critical region revealed a *Txnip* nonsense mutation in HcB-19 that is absent in its normolipidemic parental strains. *Txnip* encodes a cytoplasmic protein that binds and inhibits thioredoxin, a major regulator of cellular redox state. The mutant mice have decreased CO_2 production but increased ketone body synthesis, suggesting that altered redox status down-regulates the citric-acid cycle, sparing fatty acids for triglyceride and ketone body production. These results reveal a new pathway of potential clinical significance that contributes to plasma lipid metabolism.

For fine-mapping, we constructed a large F2 intercross between HcB-19, a recombinant congenic strain that is 88% C3H/DiSnA (C3H) and 12% C57BL/10ScSnA (B10)9[–]10, and the evolutionarily distant strain CAST/Ei. Approximately 2,700 (HcB-19 × CAST/Ei)F2 mice were generated and genotyped for 17 *Hyplip1* region microsatellite markers. Triglycerides were significantly elevated in HcB-19 (Fig. 1*a*) and yielded the highest lod score in our previously reported cross[5]. We therefore measured triglycerides for approximately one-third of (HcB-19 × CAST/Ei)F2 mice (Fig. 1*b*). Because considerable phenotypic overlap made assigning recombinant animals to a particular genotypic class difficult, we searched for additional phenotypes.

Correspondence should be addressed to A.J.L. (jlusis@mednet.ucla.edu).

In our previous cross of 183 (HcB-19 × B10)F2 animals, *Hyplip1* was linked to plasma triglycerides, LDL+VLDL cholesterol, total cholesterol and free fatty acid (FFA) amounts with lod scores of 30.5, 22.4, 10.2 and 9.2, respectively, at peak marker *D3Mit101* (ref. [5] and data not shown). As FFA levels were elevated and fatty acids are esterified to produce triglycerides or partially oxidized to form ketone bodies, we examined plasma levels of the predominant ketone body, β-hydroxybutyrate (β-HB). HcB-19 mice showed hyperketonemia, with β-HB levels increased approximately threefold (Fig. 1*c*). Plasma β-HB levels segregated with the *Hyplip1* locus in the (HcB-19 × CAST/Ei)F2 cross (Fig. 1*d*), yielding a peak lod score of 219 at *D3Mit101*, whereas triglycerides reached a lod score of 90. Notably, the variability and overlap of β-HB levels between the genotypic classes were reduced as compared with triglycerides, making the assessment of *Hyplip1* genotype for recombinant animals more definitive.

From approximately 2,700 (HcB-19 × CAST/Ei)F2 mice, we generated 184 animals with crossovers between *D3Mit76* and *D3Mit75* (Fig. 2*a*). Initial analysis restricted *Hyplip1* between *D3Mit76* and *D3Mit100* (ref. 11). We backcrossed recombinant animals to HcB-19 for progeny-testing to confirm the *Hyplip1* genotype by analysis of backcross progeny that inherited the same *Hyplip1* haplotype. To facilitate fine-mapping, we identified additional polymorphic SNP and microsatellite markers between HcB-19 and CAST/Ei (Fig. 2*b*).

We assessed the probability that a particular haplotype carried the *Hyplip1* mutation by logistic regression. We first analyzed the phenotype distribution of ketone body and triglyceride levels of nonrecombinant animals that were homozygous, heterozygous or wildtype with respect to *Hyplip1* mutant alleles between *D3Mit76* and *D3Mit100*. Using the resultant regression equations and sex-adjusted ketone body and triglyceride levels, we determined the predictive probability that the original recombinant was heterozygous [*P*(*c*/*h*)] and the predictive probabilities that backcross progeny with the same haplotype were homozygous with respect to *Hyplip1* mutant alleles [*P*(*h*/*h*)]. On the basis of four critical recombinant animals and their backcross progeny (Fig. 3), as well as additional recombinants and progeny (Table 1), the critical region was narrowed to roughly 160 kb between *D3Pds7* and *D3Pds13*. We therefore focused on this interval for physical mapping and sequencing.

To facilitate candidate gene identification, we constructed a BAC contig between *D3Mit76* and *D3Mit157* (Fig. 2*b*). We used a ‘chromosome walking’ strategy to develop a complete contig containing 128 clones and covering 3 Mb. Four BACs representing a minimum tiling path across the critical region were subcloned and sequenced, revealing 13 genes (Fig. 2*c*). Of these, only four (*Txnip*, *Rbm8*, *Pex11b*, and *Itga10*) were entirely within the maximal critical interval. We evaluated candidate genes by northern analysis and sequencing to identify possible differences between HcB-19 and its normolipidemic parental control.

Northern blot data revealed that mRNA amounts for *Txnip* were reduced approximately eightfold in HcB-19 (Fig. 4*a*). No expression differences were observed for any other genes from the locus (data not shown). Sequencing *Txnip* RT–PCR products revealed a T→A transversion in HcB-19 at position 337 in the 1,456-bp cDNA (Fig. 4*b*). This spontaneous point mutation changes a tyrosine (TAT) to a stop codon (TAA) at amino acid 97 in Txnip, which normally consists of 395 residues. Notably, this nonsense mutation in HcB-19 was absent in the C3H parental strain and 94 other strains of mice we examined (Fig. 4*b* and data not shown). In addition, by comparing over 175 kb of fully aligned, contiguous genomic sequence from HcB-19 and C3H cosmid libraries, we observed only one coding difference, the *Txnip* nonsense mutation.

The gene *Txnip* contains eight exons spanning approximately 5 kb (Fig. 2*d*). The *Hyplip1* nonsense mutation occurs in exon 2 at codon 97 (Fig. 2*d*). The *Txnip* transcript was fairly

ubiquitously expressed in all tissues examined, with the highest abundance in heart, liver and kidney (Fig. 4*c*). The decrease in *Txnip* mRNA in HcB-19 presumably results from nonsense-mediated mRNA decay through RNA surveillance mechanisms for the detection and degradation of transcripts with premature stop codons[12–13].

The *Hyplip1* nonsense mutation affects several aspects of lipid metabolism. In (HcB-19 × C57BL/6J)N4 congenic mice, plasma levels of TG, β-HB, TC, LDL+VLDL-C and FFA were significantly increased as compared with wildtype littermates (Fig. 5*a–e*). In addition, in (HcB-19 × CAST/Ei)F2 animals, the *Hyplip1* mutation was associated with increased plasma total cholesterol and LDL+VLDL cholesterol (Fig. 5*f–g*) as well as increased amounts of TG and β-HB (Fig. 1*b*,*d*), consistent with our previous cross[5]. Plasma HDL cholesterol did not segregate with *Hyplip1* (data not shown).

We previously showed that triglyceride secretion *in vivo* is increased roughly 70% in *Hyplip1* mutant mice[5]. Consistent with this, we found an approximately 70% increase in triglyceride content of HcB-19 livers (Fig. 5*i*). In addition, from isolated liver slices we observed that incorporation of ^{14}C-oleate into newly synthesized triglycerides was increased approximately 70% (Fig. 5*j*).

Hyplip1 mice have increased plasma FFA levels (Fig. 5*e*,*h*), which is predicted to increase the supply of exogenous FA to the liver because uptake is concentration-dependent. Hepatic FA are oxidized primarily in mitochondria, where they undergo complete oxidation to CO_2 via the TCA cycle, or partial oxidation to produce ketone bodies. As discussed, plasma β-HB was increased threefold in HcB-19 (Fig. 1*c*). Consistent with these findings, we observed a twofold increase in ketone body synthesis in HcB-19 liver slices (Fig. 5*k*). In contrast, CO_2 production was significantly decreased (Fig. 5*l*), demonstrating reduced oxidation by the TCA cycle. Taken together, the data indicate that *Hyplip1* results in increased FFA uptake by liver and decreased oxidation of FA by the TCA cycle, resulting in increased availability for triglyceride and ketone body synthesis. In addition, plasma lactate was significantly increased in HcB-19 mice (Fig. 5*m*), whereas plasma pyruvate was decreased (Fig. 5*n*). As the lactate: pyruvate ratio reflects [NADH]:[NAD+] concentration[14], these findings probably reflect an altered redox state resulting from the *Hyplip1* mutation in *Txnip*.

The gene *TXNIP* was first identified from HL-60 cells stimulated to differentiate into monocytes/macrophages by 1,25- dihydroxyvitamin D_3 treatment[15]. More recent work revealed that both TXNIP and Txnip bind reduced thioredoxin (TXN) *in vitro* and *in vivo* and inhibit its reducing activity[16–17]. In studies with partial proteins, amino acids 134–395 of Txnip were required for TXN binding and inhibition[17]. Because the *Hyplip1* nonsense mutation occurs at residue 97, the truncated protein will be missing crucial amino acids, resulting in misregulation of thioredoxin.

Thioredoxin is a 12-kD thiol-oxidoreductase with many cellular functions, including cell activation[18], cell growth[19], apoptosis[20], signal transduction[21] and gene expression[22]. Because Txnip inhibits thioredoxin, the *Hyplip1* mutation may cause hyperlipidemia by affecting the Txn pathway, one of the major reducing systems[23]. Alterations in redox state could explain several aspects of the hyperlipidemic phenotype. For example, increased [NADH]:[NAD+] inhibits flux through the TCA cycle and results in decreased CO_2 production[24–25]. As a result, more FA are available for the alternative oxidative pathway and for esterification.

Our results provide evidence of a new pathway with a profound influence on the regulation of lipid metabolism. Our data indicate the *Hyplip1* mutation causes a decreased flux of FA through the TCA cycle, resulting in increased availability for ketogenesis and triglyceride synthesis. Further studies are warranted to elucidate the exact molecular mechanisms by which the

Hyplip1 nonsense mutation in *Txnip* causes combined hyperlipidemia in HcB-19, as well as the potential role the human ortholog may have in FCHL or other metabolic disorders.

Methods

Mice and mouse husbandry

The development of the recombinant congenic mutant mouse strain HcB-19/*Dem* was described previously[5,9]. Because HcB-19 animals were initially unavailable, we used (HcB-19 × BALB/*c*)F1 mice for breeding to CAST/Ei mice. We genotyped the resultant progeny for polymorphic markers *D3Mit29, D3Mit76, D3Mit75* and *D3Mit121* to exclude animals with BALB/*c* alleles within or near the *Hyplip1* region. Animals with HcB-19 alleles were intercrossed to produce approximately 2,000 progeny that are essentially (HcB-19 × CAST/Ei)F2 at the *Hyplip1* locus. In addition, we generated approximately 700 (HcB-19 × CAST/Ei)F2 mice. These two groups of F2 animals are referred to as '(HcB-19 × CAST/Ei)F2' mice. We constructed (HcB-19 × C57BL/6J)N4 congenic mice by backcrossing HcB-19 to C57BL/6J for four generations and selecting for HcB-19 alleles at markers *D3Mit76* and *D3Mit101* at each generation. Heterozygous N4 mice were intercrossed to obtain progeny that we screened to identify congenic mice homozygous with respect to the *Hyplip1* nonsense mutation or wildtype. All mice were housed in groups of five or less animals per cage and maintained on a 12-h light-dark cycle at an ambient temperature of 23 °C. They were allowed *ad libitum* access to water and standard Purina Rodent Chow containing 4.5% fat (Ralston-Purina Co.).

Plasma lipid, ketone body and lactate determinations

Mice were fasted for 12 h before retro-orbital bleeding and were bled under isofluorane anesthesia 3–6 h after the beginning of the light cycle, with EDTA used as the anticoagulant. We determined plasma lipids as described previously[5]. We measured β-hydroxybutyrate levels in duplicate using a kit (#310-A, Sigma). We pre-chilled blood collection tubes on ice and centrifuged the samples within 5 min to remove erythrocytes to obtain accurate plasma lactate concentrations, which we measured in duplicate using a kit (#735-10, Sigma). For pyruvate determinations, we did not use EDTA, as whole blood was immediately deproteinized and the pyruvate measured using a kit (#726-UV, Sigma). For pyruvate measurements, we pre-chilled blood collection tubes with cold perchloric acid and kept the blood-precipitate mixture on ice for at least 5 min to ensure complete protein precipitation.

Statistical analysis

We analyzed linkage data and calculated lod scores and recombination distances using the Map Manager QT v.3.0 Program. As the triglyceride and ketone body levels of heterozygous mice overlapped with both wildtype and *Hyplip1* mutant homozygous groups, recombinant mice were evaluated statistically using logistic regression. We calculated predictive probabilities using the logistic subroutine of the SAS program (Version 6.10, 1993, SAS Institute). Given the distribution of triglyceride and ketone body levels for each genotype from animals that were nonrecombinant between markers *D3Mit76* and *D3Mit100*, we calculated logistic regression coefficients by using the ketone body values and the natural log of the triglyceride values (the natural log was used to normalize the data set.) We then used these logistic regression coefficients to calculate the probability that each parental recombinant animal was heterozygous and that each backcross progeny with the same haplotype was homozygous with respect to *Hyplip1*, given the sex-adjusted triglyceride and ketone body values. The predictive probabilities thus represent an estimate of the probability that a particular animal is heterozygous [*P*(*c*/*h*)] or homozygous [*P*(*h*/*h*)] for the *Hyplip1* mutation based on its phenotype. The total cholesterol values were highly correlated with triglycerides in this sample (r=0.8025) and inclusion of total cholesterol levels did not significantly effect the predictive

probability values after triglycerides were used in the prediction, although total cholesterol levels were significantly linked to the *Hyplip1* locus ($P<0.00005$).

Radiation hybrid mapping and genotyping

We mapped markers and genes from the *Hyplip1* region using the mouse/hamster T31 radiation hybrid panel (Research Genetics). All clone lines producing a breakpoint were typed in duplicate, as were any ambiguous typings. PCR and thermal cycling conditions were as recommended by the manufacturer. All mapping data are available at The Jackson Laboratory Mouse Radiation Hybrid database. We carried out automated genotyping of DNA microsatellite markers using fluorescent-labeled primers (Research Genetics) and ABI 377 machines according to standard protocols.

BAC contig and cosmid library construction

We identified BACs for the *Hyplip1* region by hybridizing labeled PCR products from the *Hyplip1* locus to filters from the RPCI-23 mouse BAC libraries (Children's Hospital, Oakland). Briefly, high-density filters with 10× coverage were hybridized with random-primed ^{32}P-labeled probes (1×10^6 cpm ml^{-1} hybridization solution). Ten to twenty PCR products were routinely pooled per hybridization. We pre-hybridized the filters for 1 h and then hybridized with labeled probes overnight (16–18 h) at 65 °C. We washed the filters at 65 °C for 4–6 times until all nonbound probe was essentially removed. The filters were then exposed to phosphor screens (Molecular Dynamics) for 2–24 h and analyzed on the Storm Image Analysis System (Molecular Dynamics). We interpreted the positions of positive clones according to the manufacturer's instructions, using transparent overlays as an orientation guide. The order of the markers was based on radiation hybrid mapping data and their presence or absence within each BAC clone bin. We sized BAC clones by pulsed-field gel electrophoresis. BAC ends were sequenced for primer design, PCR-amplified, and then used for chromosome walking and gap closure of the approximately 3-Mb contig we constructed between markers *D3Mit76* and *D3Mit157*. For the construction of cosmid libraries, we used fresh livers from C3H and HcB-19 mice to prepare high–molecular weight genomic DNA embedded in agarose plugs. Genomic DNA was partially digested by *Mbo*I before ligation to the pFOS1 vector that was treated with *Aat*II and *Bam*H1 (New England Biolabs). The ligated mixture was packaged using the Gigpack III xl–11 (Stratagene) according to the manufacturer's protocol and transformed into DH10B competent cells. We determined the titer of roughly 200 clones and aliquoted them into 96-well format. Row and column pools were prepared for subsequent screening. We plated several hundred colonies from each positive well, picked 1,536 colonies into four 384-well microtiter plates and then transferred the cultures onto nylon membranes for hybridization to identify individual positive clones.

Sequencing and sequence data analysis

We extracted BAC DNA using a standard cesium chloride cushion[26]. For sequencing, a sub-library in pUC18 was first constructed from each BAC clone. Briefly, we randomly sheared BAC DNA using a sonicator and end-filled with Klenow, then size-fractionated by agarose gel electrophoresis and collected fragments between 1.5 kb and 3.0 kb. We cloned the gel-purified fragments into *Sma*I-cut, bacterial alkaline phosphatase–treated pUC18. Ligation (Roche Rapid Ligation kit) and transformation of XL-10 competent cells (Stratagene) were carried out according to the manufacturer's instructions. We picked several thousand clones from each BAC library for high-throughput sequencing. We extracted plasmid DNA using the Qiagen Biorobot. Cycle sequencing was carried out using BigDye terminators (PE Applied Biosystems), purified on Centrisep spin columns in 96-well format and analyzed on an ABI 3700 capillary sequencer (PE Applied Biosystems). We purified PCR products using a kit (Qiagen) and used 30–60 ng for cycle sequencing. Raw sequence data were analyzed and

assembled using PHRED and PHRAP, and then vector and repeat sequences were masked and high-quality sequence compared to available sequence databases.

Northern-blot analysis and RT–PCR

We isolated total RNA from liver with Trizol reagent (Life Technologies) according to the manufacturer's instructions. PolyA RNA was isolated using the Oligotex mRNA kit (Qiagen), and then 2 μg was resolved by electrophoresis in a denaturing agarose gel using the NorthernMax protocol and reagents (Ambion) and transferred to Brightstar-Plus membranes (Ambion) according to the manufacturer's instructions. We labeled DNA with ^{32}P-dCTP (Amersham Pharmacia Biotech) using a random-prime kit (Life Technologies). We hybridized and washed the filters according to the NorthernMax protocol, then exposed the filters overnight and imaged them using the Storm Image Analysis System (Molecular Dynamics). We carried out RT–PCR on total RNA using the Access RT–PCR kit (Promega).

Metabolism of ^{14}C-oleate in liver slices

After an overnight fast, mice were anesthetized with pentobarbital (50 mg kg^{-1}) and the liver removed. We used a Staddie-Riggs microtome to obtain fresh liver slices (~0.5 mm thick) that were immediately weighed and incubated for 1 h under 95% O_2:5% CO_2 in Krebs-Henseleit buffer containing 5.5 mM glucose and a 3% BSA/1 mM ^{14}C-oleic acid complex[27]. The final specific activity was 250,000 dpm μmol^{-1}. We determined $^{14}CO_2$ production using hyamine hydroxide to trap the CO_2 and measuring the radioactive counts in a liquid scintillation spectrometer essentially as described[27]. The ^{14}C-oleic acid incorporation into ketone bodies and secreted triglycerides was determined in the liver slice incubations under similar conditions, except the cells were continuously gassed with 95% O_2:5% CO_2 and no hyamine hydroxide was used. After the 40-min incubation, we removed the media for extraction of lipids and ketone bodies. We measured the radioactivity incorporated into ketone bodies after perchloric acid deproteinization as described[27]. The triglycerides were separated from media lipid extracts by thin layer chromatography, and the radioactivity in the band corresponding to triglycerides was determined as previously described[28].

Primers

Primers for SNP and microsatellite markers are available upon request.

Genbank accession number

The accession number for the *Hyplip1* cosmid sequence is AF449447. The accession number for the *Txnip* cDNA is AF173681.

Acknowledgments

This work was supported by grants from the National Institutes of Health and the UCLA Laubisch Fund (A.J.L.) and by a USPHS National Research award (J.B.). We thank S. Charugundla for help in the plasma lipid determinations. We appreciate the excellent technical assistance of Y. Lee, D. San Juan, L. Chen, A. Cairo, S. Tobias, K. Amburgey, D. Civello, J. Choi and Q. Zhang. We also thank O. Iakoubova, H. Sakul and R. Woychik for their expert advice. We appreciate the aid of J. Sinsheimer for the statistical analysis of recombinant animals. We are grateful to R. Davis for his comments on this manuscript. We also thank L. Peltonen, P. Pajukanta, H. Allayee and K. Krass for thoughtful discussion and input. Production of HcB-19/Dem was supported by grants from the Dutch Cancer Foundation and the European Commission (P.D.).

References

1. Genest JJ Jr, et al. Familial lipoprotein disorders in patients with premature coronary artery disease. Circulation 1992;85:2025–2033. [PubMed: 1534286]

2. Grundy SM, Chait A, Brunzell JD. Familial combined hyperlipidemia workshop. Arteriosclerosis 1987;7:203–207.
3. Goldstein JL, Schrott HG, Hazzard WR, Bierman EL, Motulsky AG. Hyperlipidemia in coronary heart disease. II. Genetic analysis of lipid levels in 176 families and delineation of a new inherited disorder, combined hyperlipidemia. J. Clin. Invest 1973;52:1544–1568. [PubMed: 4718953]
4. Nikkila EA, Aro A. Family study of serum lipids and lipoproteins in coronary heart-disease. Lancet 1973;1:954–959. [PubMed: 4121585]
5. Castellani LW, et al. Mapping a gene for combined hyperlipidaemia in a mutant mouse strain. Nature Genet 1998;18:374–377. [PubMed: 9537422]
6. Pajukanta P, et al. Linkage of familial combined hyperlipidaemia to chromosome 1q21–q23. Nature Genet 1998;18:369–373. [PubMed: 9537421]
7. Pei W, et al. Support for linkage of familial combined hyperlipidemia to chromosome 1q21–q23 in Chinese and German families. Clin. Genet 2000;57:29–34. [PubMed: 10733233]
8. Coon H, et al. Replication of linkage of familial combined hyperlipidemia to chromosome 1q with additional heterogeneous effect of apolipoprotein A-I/C-III/ A-IV locus. The NHLBI family heart study. Arterioscler. Thromb. Vasc. Biol 2000;20:2275–2280. [PubMed: 11031215]
9. Demant P, Hart AA. Recombinant congenic strains–a new tool for analyzing genetic traits determined by more than one gene. Immunogenetics 1986;24:416–422. [PubMed: 3793154]
10. Groot PC, et al. The recombinant congenic strains for analysis of multigenic traits: genetic composition. FASEB J 1992;6:2826–2835. [PubMed: 1634045]
11. Pajukanta P, et al. Fine mapping of *Hyplip1* and the human homolog, a potential locus for FCHL. Mamm. Genome 2001;12:238–245. [PubMed: 11252174]
12. Culbertson MR. RNA surveillance. Unforeseen consequences for gene expression, inherited genetic disorders and cancer. Trends Genet 1999;15:74–80. [PubMed: 10098411]
13. Leeds P, Peltz SW, Jacobson A, Culbertson MR. The product of the yeast *UPF1* gene is required for rapid turnover of mRNAs containing a premature translational termination codon. Genes Dev 1991;5:2303–2314. [PubMed: 1748286]
14. Williamson DH, Lund P, Krebs HA. The redox state of free nicotinamide-adenine dinucleotide in the cytoplasm and mitochondria of rat liver. Biochem. J 1967;103:514–527. [PubMed: 4291787]
15. Chen KS, DeLuca HF. Isolation and characterization of a novel cDNA from HL-60 cells treated with 1,25-dihydroxyvitamin D-3. Biochim. Biophys. Acta 1994;1219:26–32. [PubMed: 8086474]
16. Nishiyama A, et al. Identification of thioredoxin-binding protein-2/vitamin D(3) up-regulated protein 1 as a negative regulator of thioredoxin function and expression. J. Biol. Chem 1999;274:21645–21650. [PubMed: 10419473]
17. Junn E, et al. Vitamin D_3 up-regulated protein 1 mediates oxidative stress via suppressing the thioredoxin function. J. Immunol 2000;164:6287–6295. [PubMed: 10843682]
18. Yodoi J, Uchiyama T. Diseases associated with HTLV-1: virus, IL-2 receptor dysregulation and redox regulation. Immunol. Today 1992;13:405–411. [PubMed: 1418377]
19. Gasdaska JR, Berggren M, Powis G. Cell growth stimulation by the redox protein thioredoxin occurs by a novel helper mechanism. Cell Growth Differ 1995;6:1643–1650. [PubMed: 9019170]
20. Ueda S, et al. Redox regulation of caspase-3(-like) protease activity: regulatory roles of thioredoxin and cytochrome c. J. Immunol 1998;161:6689–6695. [PubMed: 9862698]
21. Nakamura H, Nakamura K, Yodoi J. Redox regulation of cellular activation. Annu. Rev. Immunol 1997;15:351–369. [PubMed: 9143692]
22. Hirota K, et al. AP-1 transcriptional activity is regulated by a direct association between thioredoxin and Ref-1. Proc. Natl Acad. Sci. USA 1997;94:3633–3638. [PubMed: 9108029]
23. Holmgren A. Thioredoxin and glutaredoxin systems. J. Biol. Chem 1989;264:13963–13966. [PubMed: 2668278]
24. LaNoue KF, Bryla J, Williamson JR. Feedback interactions in the control of citric acid cycle activity in rat heart mitochondria. J. Biol. Chem 1972;247:667–679. [PubMed: 4333508]
25. Kimura RE, Warshaw JB. Control of fatty acid oxidation by intramitochondrial [NADH]/[NAD+] in developing rat small intestine. Pediatr. Res 1988;23:262–265. [PubMed: 3353171]

26. Sambrook, J.; Fritsch, EF.; Maniatis, T. Molecular Cloning: A Laboratory Manual. 2nd ed. New York: Cold Spring Harbor Laboratory Press; 1989.

27. Olubadewo JO, Heimberg M. Effects of adrenergic agonists and antagonists on the metabolism of [1-^{14}C] oleic acid by rat hepatocytes. Biochem. Pharmacol 1993;45:2441–2447. [PubMed: 8328982]

28. Castellani LW, Wilcox HC, Heimberg M. Relationships between fatty acid synthesis and lipid secretion in the isolated perfused rat liver: effects of hyperthyroidism, glucose and oleate. Biochim. Biophys. Acta 1991;1086:197–208. [PubMed: 1932102]

29. Doolittle MH, Wong H, Davis RC, Schotz MC. Synthesis of hepatic lipase in liver and extrahepatic tissues. J. Lipid Res 1987;28:1326–1334. [PubMed: 3323389]

30. Lanford, RE.; Estlack, L. A cultivation method for highly differentiated primary chimpanzee hepatocytes permissive for hepatitis C virus replication. In: Lau, JYN., editor. Methods in Molecular Medicine: Hepatitis C Protocols. New Jersey: Humana, Totowa; 1998. p. 501-515.

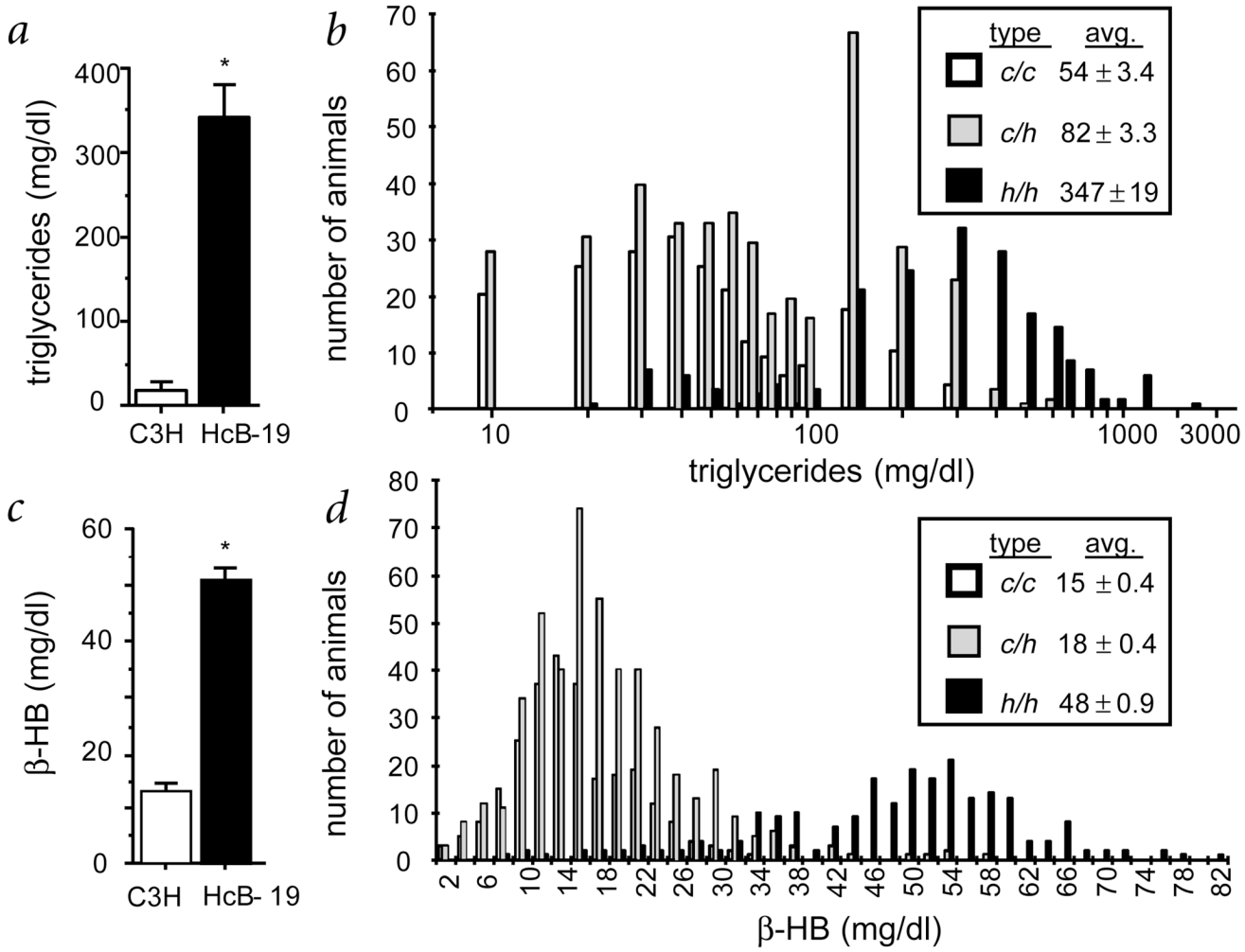

Fig. 1.

Distributions of triglyceride and ketone body levels. ***a***, Plasma levels of triglycerides in HcB-19 and its C3H parental control. The average ± s.e.m. is shown for six animals in each group. Asterisk indicates $P<0.0001$. ***b***, Distribution of plasma triglycerides in (HcB-19 × CAST/Ei) F2 mice grouped by genotype at *D3Mit101* so that each group represents animals with triglycerides within a certain interval (for example, the group at 30 represents animals with triglycerides from 21–30 mg dl^{-1}). Filled bars indicate values for animals homozygous with respect to HcB-19 alleles (*h/h*), hatched bars indicate heterozygote values (*c/h*) and open bars denote values for animals homozygous with respect to wildtype CAST/Ei alleles (*c/c*). The genotype and average triglyceride value ± s.e.m. (avg.) in mg dl^{-1} for each group are indicated in the legend box. *N*=259 wildtype, 489 heterozygote and 214 homozygote animals. *c*, Plasma levels of ketone body β-hydroxybutyrate in the HcB-19 mouse and its C3H parent control. The average ± s.e.m. is shown for six animals in each group. Asterisk indicates $P<0.0001$. *d*, Distribution of plasma levels of ketone body β-hydroxybutyrate in (HcB-19 × CAST/Ei)F2 mice grouped by genotype at *D3Mit101* so that each group represents animals with plasma ketone body levels within a certain interval (for example, the group at 30 represents animals with ketone bodies from 29–30 mg dl^{-1}). *N*=259 wildtype, 489 heterozygote and 214 homozygote animals. Abbreviations and designations are identical to panel *b*.

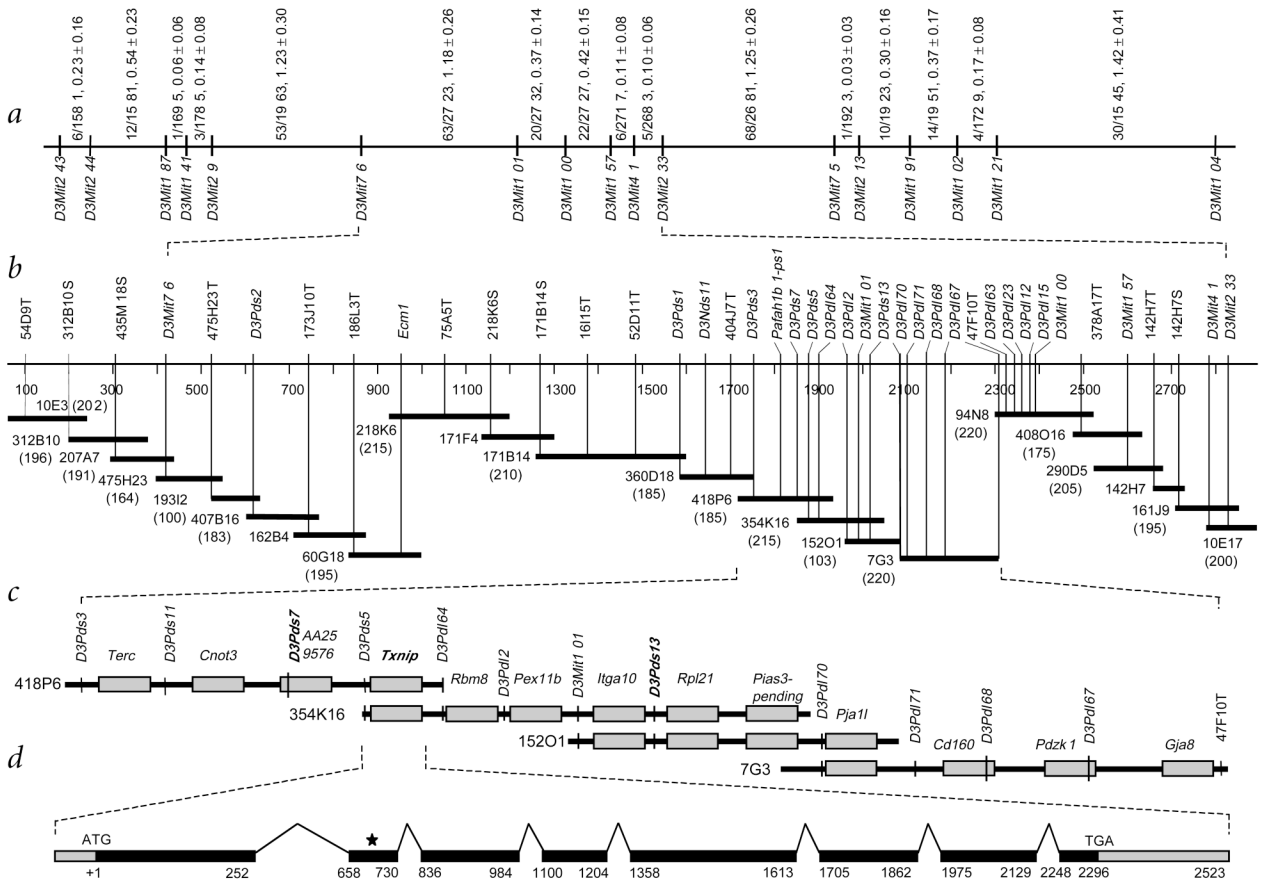

Fig. 2.

Physical- and fine-mapping of the *Hyplip1* locus. ***a***, Fine-mapping of (HcB-19 × CAST/Ei)F2 animals by genotyping 17 microsatellite markers. The ratios of the number of recombinants to the total number of informative mice plus the recombination frequencies ± s.e.m. (in cM) are shown. ***b***, The minimum tiling path of the BAC contig for the *Hyplip1* locus. Solid black lines represent 22 individual BAC clones. The BAC clone name is listed, and the BAC size in kb (when known) is given in parenthesis. Markers, genes, and BAC end clone sequences are shown at the top, and the estimated physical distances (in kb) are given. The limiting breakpoint markers that define the maximal location of the gene *Hyplip**1*** are in boldface. ***c***, Four overlapping BACs from the *Hyplip1* locus that were subcloned and sequenced to identify 13 candidate genes. Each BAC clone name is given; gray boxes depict genes. The approximate positions of microsatellite markers and SNPs are shown. The *Hyplip1* gene (*Txnip*) and the markers that define the maximal location of *Hyplip1* are shown in boldface. ***d***, Genomic structure of *Hyplip1* (*Txnip*). Solid black lines indicate the eight exons of *Txnip*, and an asterisk indicates the location of the T→A nonsense mutation observed in strain HcB-19. Numbers listed below the figure indicate the DNA base positions of the exon-intron junctions.

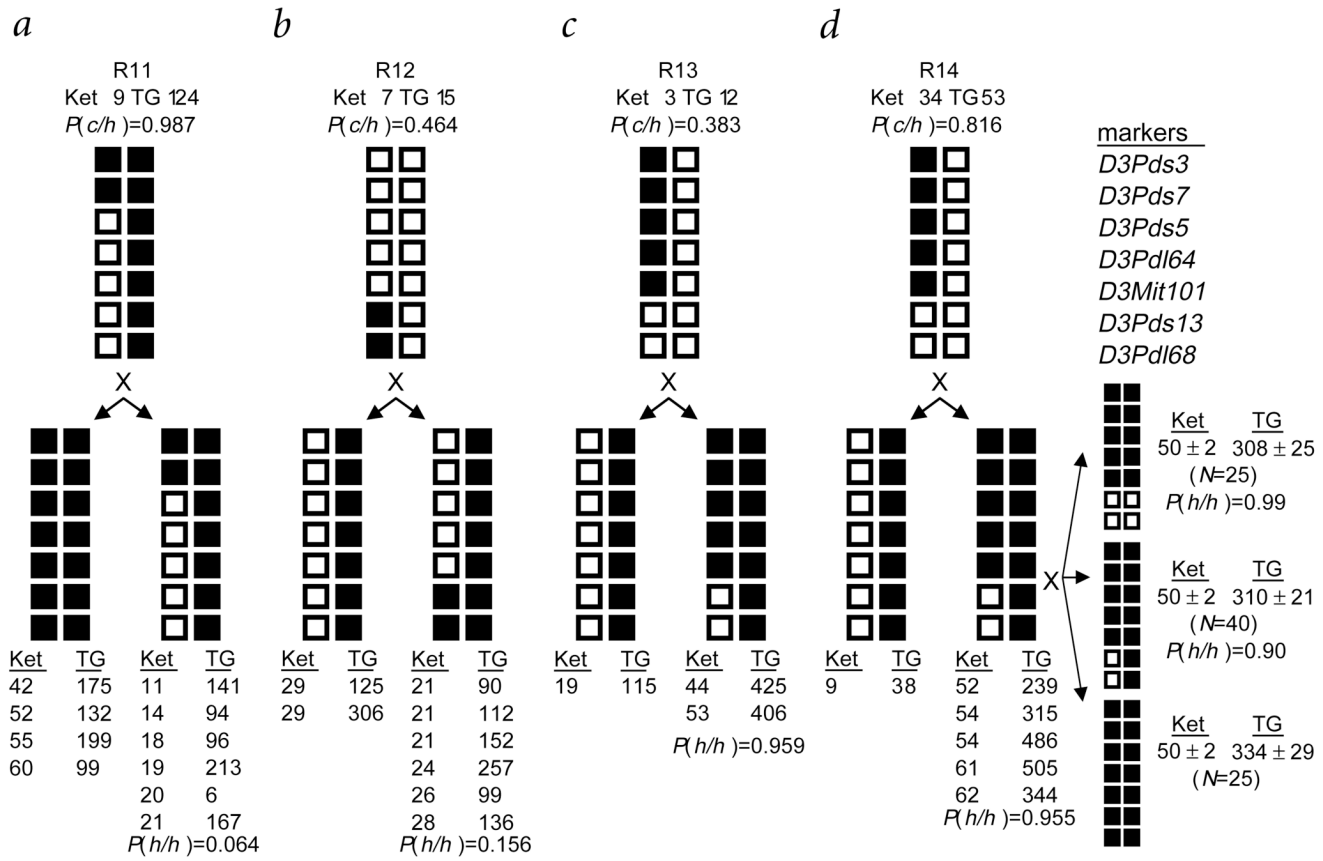

Fig. 3.

Recombinant animals and their HcB-19 backcross progeny that define the maximal critical interval containing *Hyplip1*. ***a***, Recombinant R11 and 10 backcross progeny. Backcross mice are grouped according to the inheritance of a recombinant or nonrecombinant haplotype across the *Hyplip1* locus for the seven markers listed at the right. Filled boxes indicate HcB-19 (*h*) alleles and open boxes denote CAST/Ei (*c*) alleles. Ketone body (Ket) and triglyceride (TG) levels in mg dl^{-1} are given for each parental recombinant and their progeny. The predictive probability of heterozygosity, *P*(*c/h*), is shown for each parental recombinant, and the average predictive probability of homozygosity, *P*(*h/h*), is given for backcross progeny with the same haplotype. The R11 recombinant and all six backcross progeny with the same haplotype have lower β-HB and TG levels as compared with littermates homozygous with respect to HcB-19 alleles. R11 had a high probability of being heterozygous [*P*(*c/h*)=0.987] and the backcross progeny had a low probability of homozygosity with respect to *Hyplip1* [*P*(*h/h*)=0.064], indicating that *Hyplip1* is distal to *D3Pds7*. ***b***, Recombinant R12 and 8 backcross progeny. All six backcross progeny with the parental haplotype have normal β-HB and TG levels, with a low probability of homozygosity with respect to *Hyplip1* [*P*(*h/h*)=0.156]. Thus, *Hyplip1* lies proximal to *D3Pds13*. ***c***, Recombinant R13 and 3 backcross progeny. As shown, R13 carries *Hyplip1* alleles proximal to *D3Pds13*. Backcross progeny carrying this crossover have increased amounts of β-HB and TG, indicating homozygosity for *Hyplip1* with a high probability [*P*(*h/h*)=0.959], giving further evidence that *Hyplip1* is proximal to *D3Pds13*. ***d***, Recombinant R14, six backcross progeny, and 90 animals obtained from intercrossing backcross progeny with the crossover breakpoint. R14 had a high probability of being heterozygous [*P*(*c/h*)=0.816]. Backcross progeny with the same haplotype have increased amounts of β-HB and TG, indicating homozygosity with respect to *Hyplip1* [*P*(*h/h*)=0.955].

When these mice are intercrossed, all resultant progeny have increased β-HB and TG levels (the average ± s.e.m. for each genotypic group is shown), providing additional evidence for placing the distal boundary for *Hyplip1* at *D3Pds13*.

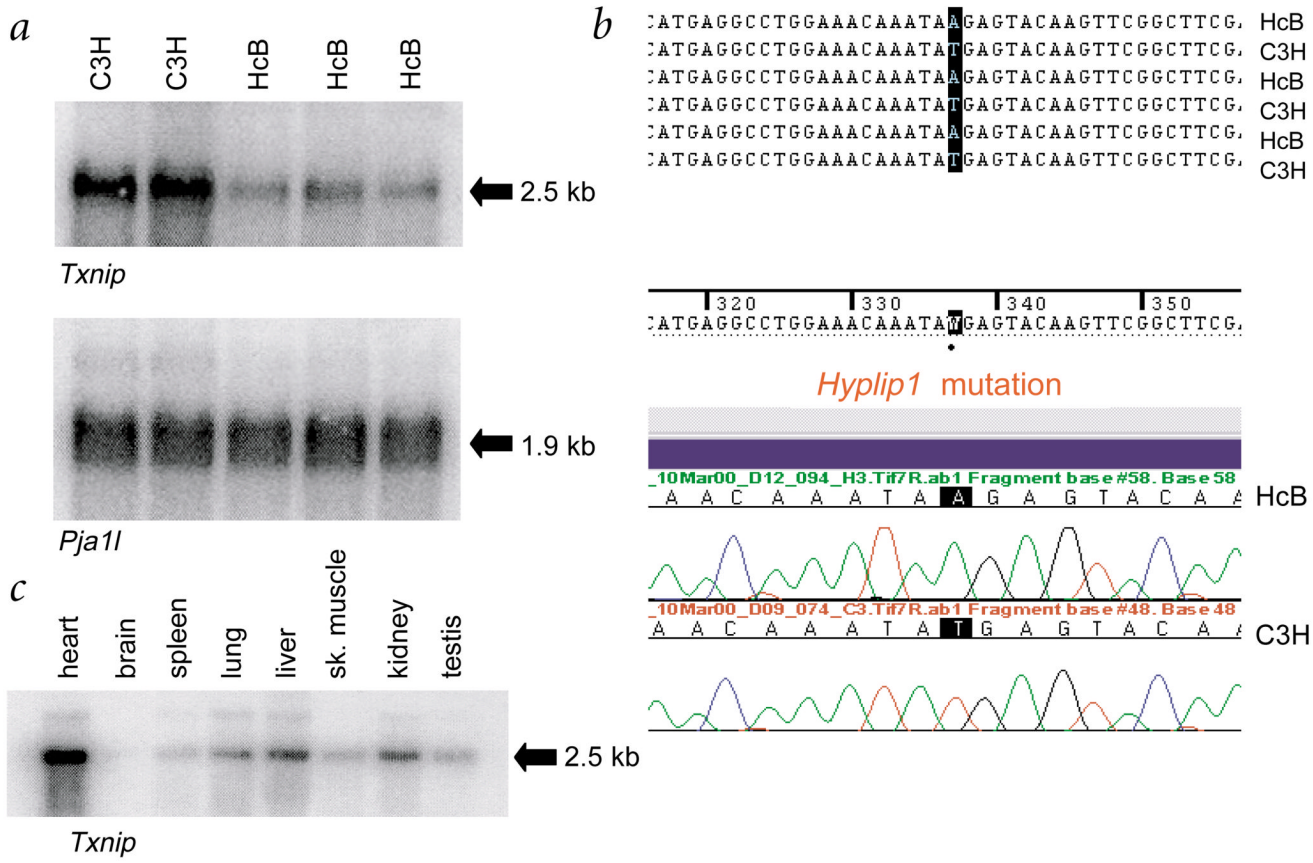

Fig. 4.

Expression and sequence analysis of *Txnip*. ***a***, Northern blot data revealing decreased mRNA expression for *Txnip* in HcB-19 as compared with the C3H parental control strain. Expression levels for another gene from the *Hyplip1* region, *Pja1l*, serve as a locus and RNA loading control. ***b***, Sequence analysis of HcB-19 and C3H mice reveals a T→A transversion mutation present in HcB-19 that is absent from the C3H strain from which it was derived. The sequence chromatograms from HcB-19 and C3H mice are shown, as well as the DNA sequence data from three HcB-19 and three C3H mice. ***c***, Northern-blot analysis of the *Txnip* transcript in various tissues reveals detectable expression in brain, spleen, lung, liver, skeletal muscle, kidney and testis, with the highest abundance occurring in heart.

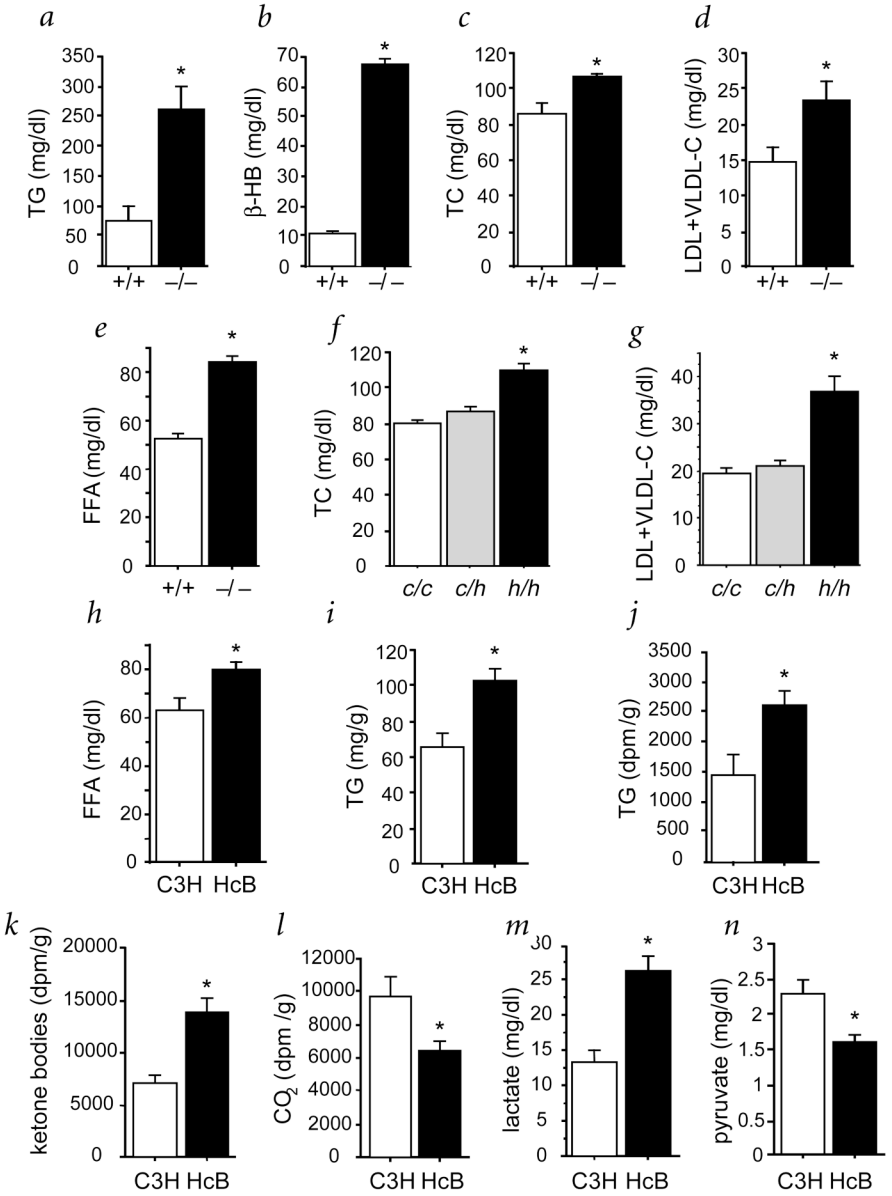

Fig. 5.

Metabolic consequences of the *Hyplip1* nonsense mutation in *Txnip*. ***a***, Plasma triglycerides for (HcB-19 × C57BL/6J)N4 congenic mice homozygous (−/−) or wildtype (+/+) for the *Hyplip**1*** nonsense mutation. *N*=6 animals in each group. Asterisk indicates *P*<0.005. ***b***, Plasma β-hydroxybutyrate levels for (HcB-19 × C57BL/6J)N4 congenic mice. *N*=6 animals in each group. Asterisk indicates *P*<0.0001. ***c***–***e***, Plasma levels for total cholesterol (*c*), LDL+VLDL cholesterol (*d*) and free fatty acids (*e*) for (HcB-19 × C57BL/6J)N4 congenic mice. *N*=6 animals in each group. Asterisk indicates *P*<0.05. ***f***,***g***, Plasma levels for total cholesterol (*f*) and LDL +VLDL cholesterol (*g*) for (HcB-19 × CAST/Ei)F2 animals grouped by genotype at marker *D3Mit101*. *N*=124 wildtype (*c*/*c*), 273 heterozygote (*c*/*h*) and 113 animals homozygous (*h*/*h*) with respect to *Hyplip1* mutant alleles. Asterisk indicates *P*<0.00005. ***h***, Plasma free fatty acid levels for nine HcB-19 (HcB) and nine C3H controls. Asterisk indicates *P*<0.01. ***i***, Total hepatic triglyceride content (in mg per g of liver tissue) from HcB-19 and C3H livers that were perfused to remove plasma lipids. *N*=4 C3H animals and 5 HcB-19 animals. Asterisk indicates *P*<0.01.

j, Dpm of ^{14}C-oleic acid per g of liver tissue in newly-synthesized triglycerides secreted from liver slices isolated from fasted HcB-19 and C3H mice. *N*=6 animals in each group. Asterisk indicates *P*<0.05. ***k***, Amount of newly-synthesized ketone bodies (in dpm per g of liver tissue) from isolated liver slices. *N*=5 C3H and 6 HcB-19 animals. Asterisk indicates *P*<0.005. ***l***, Amount of newly-synthesized CO_2 (in dpm per g of liver tissue) from isolated liver slices. *N*=4 C3H and 5 HcB-19 animals. Asterisk indicates *P*<0.05. ***m***, Plasma lactate levels (in mg dl^{-1}) from HcB-19 and C3H mice. Asterisk indicates *P*<0.001. *N*=5 animals in each group. ***n***, Pyruvate levels (in mg dl^{-1}) from whole blood from HcB-19 and C3H mice. Asterisk indicates *P*<0.008. *N*=5 animals in each group.

Nat Genet. Author manuscript; available in PMC 2010 March 29.

Table 1

Select informative recombinant animals and their backcross progeny

ID# mg/dl	Ket mg/dl	TG Breakpoint	Crossover	Genotype P(c/h)	Pred Prob Prog	No. of mg/dl	Avg Ket. mg/dl	Avg TG P(h/h)	Avg
1	82	1063	*D3Pds1–D3Pds3*	c/h-h/h	0.00001	15	53 ± 3	339 ± 51	0.924
2	44	218	*D3Pds1–D3Pds3*	c/h-h/h	0.056	11	52 ± 3	378 ± 45	0.975
3	54	980	*D3Pds1–D3Pds3*	c/h-h/h	0.012	3	53 ± 3	157 ± 37	0.962
4	17	27	*D3Pds1–D3Pds3*	c/c-c/h	0.635	7	56 ± 3	276 ± 50	0.975
5	6	98	*D3Pds1–D3Pds3*	h/h-c/h	0.994	1	23	240	0.152
6	26	19	*D3Pds1–D3Pds3*	h/h-c/h	0.966	4	17 ± 4	118 ± 20	0.058
7	25	28	*D3Pds1–D3Pds3*	h/h-c/h	0.961	6	22 ± 2	86 ± 23	0.094
8	18	36	*D3Pds1–D3Pds3*	h/h-c/h	0.978	2	22 ± 3	7 ± 5	0.051
9	8	71	*D3Pds1–D3Pds3*	c/h-c/c	0.575	15	13 ± 1	142 ± 21	0.023
10	44	147	*D3Pds7–D3Pds5*	c/h-h/h	0.080	0	–	–	–
11	9	124	*D3Pds7–D3Pds5*	h/h-c/h	0.987	6	17 ± 2	120 ± 29	0.064
12	7	15	*D3Mit101–D3Pds13*	c/c-c/h	0.464	6	24 ± 1	141 ± 25	0.156
13	3	12	*D3Mit101–D3Pds13*	c/h-c/c	0.383	2	49 ± 4	416 ± 10	0.959
14	34	53	*D3Mit101–D3Pds13*	c/h-c/c	0.816	70	51 ± 1	305 ± 15	0.946
15	ND	ND	*D3Pds13–D3Pdl68*	c/h-h/h	–	6	20 ± 1	88 ± 13	0.062
16	60	227	*D3Pdl70–D3Pdl71*	h/h-c/h	0.003	0	–	–	–
17	40	470	*D3Pdl67–D3Pdl63*	h/h-c/h	0.058	0	–	–	–
18	ND	ND	*D3Pdl67–D3Pdl63*	c/h-c/c	–	12	52 ± 3	501 ± 93	0.949
19	22	97	*D3Pdl23–D3Pdl12*	c/h-c/c	0.773	5	51 ± 4	294 ± 42	0.960
20	9	133	*D3Mit100–D3Mit157*	c/h-h/h	0.986	8	19 ± 3	137 ± 36	0.075
21	49	207	*D3Mit100–D3Mit157*	h/h-c/h	0.024	6	38 ± 4	365 ± 92	0.773
22	19	49	*D3Mit100–D3Mit157*	c/h-c/c	0.701	40	49 ± 2	405 ± 29	0.890
23	ND	ND	*D3Mit100–D3Mit157*	c/h-c/c	–	8	60 ± 3	468 ± 63	0.995

The ketone body value (Ket), triglycerides (TG), breakpoint, genotype, predictive probability of heterozygosity [*P*(*c*/*h*)] and number of recombinant backcross progeny are given for each recombinant animal. The average ± s.e.m. (Avg) for ketone bodies, triglycerides, and predictive probabilities of being homozygous for *Hyplip1* [*P*(*h*/*h*)] are listed for all backcross animals that inherited the recombinant chromosome. ND, not determined; *h*/*h*, homozygous HcB-19 alleles; *c*/*c*, homozygous CAST/Ei alleles; *c*/*h*, heterozygous.